Cytometry Part A 59A:237–245 (2004)

Distinguishing Modes of Cell Death Using the ImageStream® Multispectral Imaging Flow Cytometer

Thaddeus C. George,* David A. Basiji, Brian E. Hall, David H. Lynch, William E. Ortyn, David J. Perry, Michael J. Seo, Cathleen A. Zimmerman, and Philip J. Morrissey
Amnis® Corporation, Seattle, Washington

Received 16 December 2003; Revision Received 27 February 2004; Accepted 28 February 2004

Background: Here we demonstrate the ability of the ImageStream® 100 Multispectral Imaging Cytometer to discriminate between live, necrotic, and early and late apoptotic cells, using unique combinations of photometric and morphometric features.
Methods: Live, necrotic, and early and late apoptotic cells were prepared and analyzed by immunofluorescence microscopy, conventional flow cytometry, and imaging flow cytometry, both as single populations and as a heterogeneous mixture of cells.
Results: Live (annexin V^-, 7-AAD^-) and early apoptotic (annexin V^+, 7-AAD^-) cells were readily identifiable using either conventional or ImageStream based flow cytometric methods. However, inspection of multispectral images of cells demonstrated that the annexin V^+, 7-AAD^+ population contained both necrotic and late-stage apoptotic cells. Although these cells could not be distinguished using conventional flow cytometric techniques, they were separable using unique combinations of photometric and morphometric measures available using ImageStream technologies.
Conclusions: Using multispectral imagery, morphologically distinct cell populations can be distinguished using features not available with conventional flow cytometers. In particular, the ability to couple morphometric with photometric measures makes it possible to distinguish live cells from cells in the early phases of apoptosis, as well as late apoptotic cells from necrotic cells. © 2004 Wiley-Liss, Inc.

Key terms: multispectral imaging cytometry; apoptosis; necrosis; photometrics; morphometrics

Apoptosis is a complex, tightly-regulated process by which a cell orchestrates its own destruction in response to specific internal or external triggers (1,2) and proceeds in a manner that is designed to prevent damage to surrounding cells and tissues. Apoptotic cells typically appear shrunken, with condensed chromatin and fragmented nuclei. Although plasma membrane integrity is initially preserved, in later stages the plasma membrane becomes compromised and the cells shed apoptotic bodies consisting of organelles and cytoplasm and/or nuclear fragments. Apoptotic cells are rapidly phagocytosed and eliminated in vivo, thus preventing the induction of inflammatory responses; this process is critical to the maintenance of tissue and immune cell development and homeostasis (1–3). Inappropriately low apoptotic rates can result in cancer or autoimmune disease, while high rates can result in neurodegenerative disease or immunodeficiency (4–6). In contrast, necrotic cell death is a largely unregulated process in which the cells generally have intact nuclei with limited chromatin condensation. Cells undergoing necrosis do not induce an early phagocytic response. Instead, the cells swell and rupture, and the release of cellular contents can result in significant local tissue damage and inflammation (1).

Research aimed at cell death regulation has produced a number of methods to identify and quantify apoptotic cells, and to distinguish between cells undergoing apoptosis versus necrosis. Among these, flow cytometry has become a commonly used tool in the identification and quantification of apoptosis. Changes in cell size, shape,

Contract grant sponsor: NIH; Contract grant numbers: 9 R44 CA01798-02, 1 R43 GM58956-01.
Development of the ImageStream technology was partially supported by the NIH grants indicated.
*Correspondence to: Thaddeus C. George, Amnis Corp., 2505 Third Ave, Suite 210, Seattle, WA 98121.
E-mail: t.george@Amnis.com
Published online 17 May 2004 in Wiley InterScience (www.interscience.wiley.com).
DOI: 10.1002/cyto.a.20048

and granularity associated with apoptosis can be inferred from scattered laser light (7). Early intracellular events, such as the loss of the mitochondrial inner membrane potential or activation and the cleavage of caspases, can also be detected using electropotential sensitive dyes (8–12) or fluorogenic substrates (13–15). Another early apoptotic event results in exposure of phosphatidylserine on the outer surface of the plasma membrane, which can be detected by fluorochrome-labeled annexin V (16–19). Apoptotic cells eventually lose the ability to exclude cationic nucleotide-binding dyes, and nuclear DNA is stained with dyes such as propidium iodide and 7-aminoactinomycin D (7-AAD) (15,20–23). Other techniques that can be used to identity apoptosis include biochemical identification of the activated proteases (e.g., caspases, poly (ADP-ribose) polymerase), release of mitochondrial cytochrome c, quantification of cellular DNA content, and progressive endonucleolytic cleavage of nuclear DNA (24–28).

As noted above, conventional flow cytometric methods do not provide direct morphologic evidence of cell death. Rather, these techniques usually target molecular changes that are associated with apoptosis. However, such changes are not always specific to apoptosis and may also be present in cells undergoing necrotic death (15,29,30). For example, necrotic cells, like advanced apoptotic cells, stain with both annexin V and 7-AAD (15,29). Thus, visualization of the characteristic morphologic changes associated with apoptosis is still considered to be absolutely necessary for its identification (1,31). Standard microscopic techniques allow visualization of specific molecular and biochemical changes associated with apoptosis and also morphologic changes that distinguish apoptosis from necrosis. However, they also require subjective and time-consuming image viewing and processing of relatively limited numbers of cells that make statistically valid comparisons difficult (32). Thus, the need exists for techniques that can provide the statistical power offered by flow cytometry, coupled with the critical assessment capabilities associated with microscopic analysis. Beyond simply the analysis of apoptosis and necrosis, interest in the dynamic nature of the living cell and efforts to model cell processes (variously termed "cytomics" or "systems biology") are powerful drivers for new techniques to acquire ever more comprehensive data from cells and cell populations, as Valet, Leary, and Tárnok describe in the Introduction to this special issue of *Cytometry* (36).

We have recently developed methodologies for simultaneous high-speed multispectral imaging of cells in brightfield, darkfield, and four channels of fluorescence in flow (33,34). Using both photometric and morphometric features derived from the multimode imagery, it is now possible to discriminate cell types and features in heterogeneous populations of cells, including both nonadherent and adherent cell types. In this study, we demonstrate the ability to discriminate between live cells, necrotic cells, and cells in both the early and late stages of apoptosis using unique combinations of features provided in the ImageStream® Multispectral Imaging Cytometer and the IDEAS® data analysis software.

MATERIALS AND METHODS:
Instrumentation

Figure 1 illustrates the layout and key components of the ImageStream platform. Cells are hydrodynamically focused into a core stream and orthogonally illuminated for both darkfield (analogous to side scatter) and fluorescence imaging. The cells are simultaneously transilluminated via a spectrally-limited source (e.g., filtered white light or a light emitting diode) for brightfield imaging. Light is collected from the cells with an imaging objective lens and is projected on a charge-coupled detector (CCD) . The optical system has a numeric aperture of 0.75 and the CCD pixel size in object space is 0.5 μm^2, allowing high resolution imaging at event rates of approximately 100 cells per second. Each pixel is digitized with 10 bits of intensity resolution, providing a minimum dynamic range of three decades per pixel. In practice, the spread of signals over multiple pixels results in an effective dynamic range that typically exceeds four decades per image. Additionally, the sensitivity of the CCD can be independently controlled for each multispectral image, resulting in a total of approximately six decades of dynamic range across all the images associated with an object.

Prior to projection on the CCD, the light is passed through a spectral decomposition optical system that directs different spectral bands to different lateral positions across the detector (33). With this technique, an image is optically decomposed into a set of six subimages, each corresponding to a different color component, and spatially isolated from the remaining subimages. This process allows for identification and quantitation of signals within the cell by physically separating on the detector signals that may originate from overlapping regions of the cell. Spectral decomposition also allows multimode imaging: the simultaneous detection of brightfield, darkfield, and multiple colors of fluorescence. This is illustrated in Figure 1, which depicts a red brightfield illumination source and the associated transmitted light images in the red detector channel adjacent to fluorescent and scattered light images in the other spectral channels. The process of spectral decomposition occurs during the image formation process rather than via digital image processing of a conventional composite image.

The CCD is operated using a technique called time-delay-integration (TDI), a specialized detector readout mode that preserves sensitivity and image quality even with fast relative movement between the detector and the objects being imaged. As with any CCD, image photons are converted to photocharges in an array of pixels. However, in TDI operation, the photocharges are continuously shifted from pixel to pixel down the detector, parallel to the axis of flow. If the photocharge shift rate is synchronized with the velocity of the flowing cell's image, the effect is similar to physically panning a camera: image streaking is avoided despite signal integration times that are orders of magnitude longer than in conventional flow cytometry. The current instrument operates at a continuous data rate of approximately 30 megapixels per second

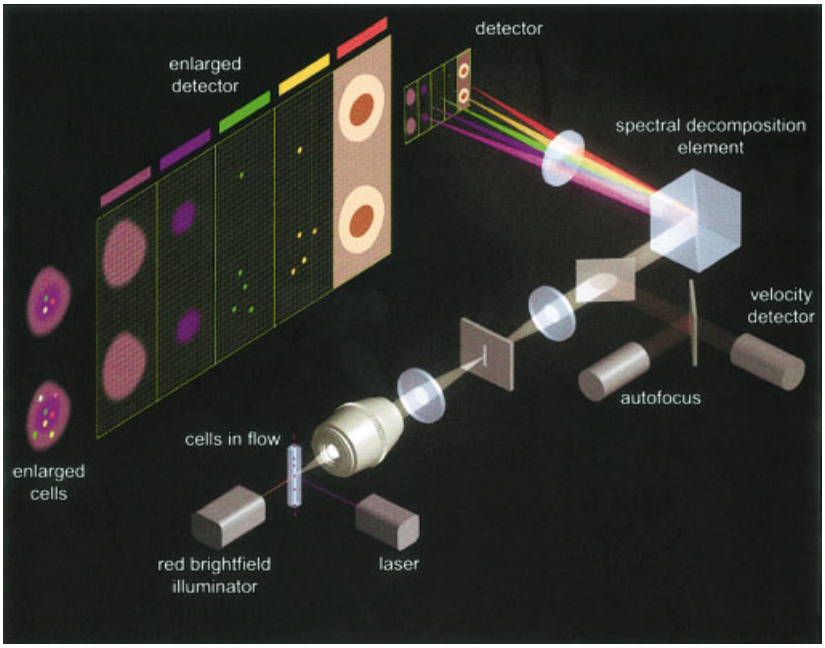

FIG. 1. Schematic representation of the ImageStream 100 multispectral imaging cytometer. Described in detail in Materials and Methods.

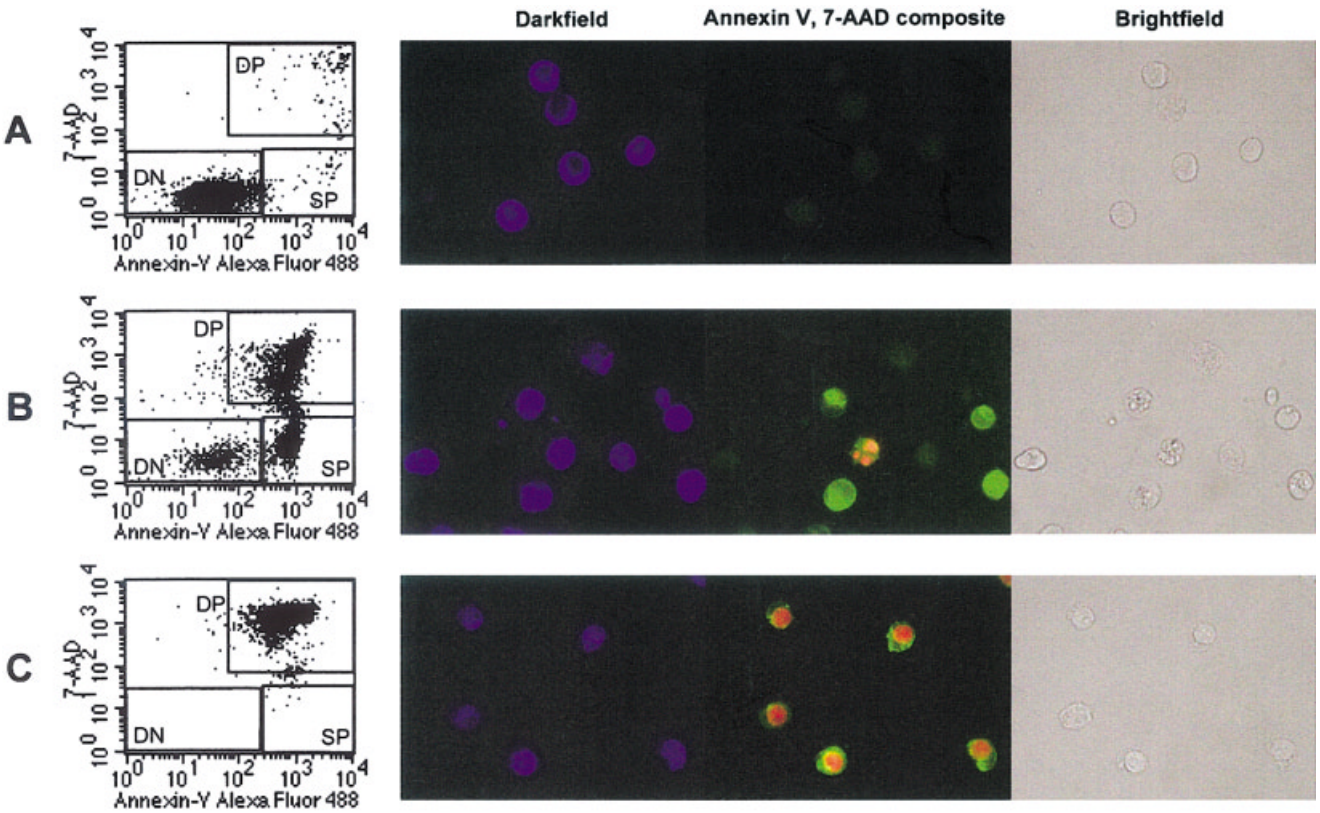

FIG. 2. Analysis of cell death using standard flow cytometry and immunofluorescence microscopy. Untreated Jurkat cells (**A**), Jurkat cells treated with 1 μM CPT for 18 h (**B**) or Jurkat cells treated with 0.3% hydrogen peroxide for 1 h (**C**) were stained with Alexa Fluor 488 conjugated annexin V and 7-AAD. Cells were analyzed either by conventional flow cytometry (using a BD FACSort™) or visualized on slides using a Nikon Eclipse E600 fluorescence microscope equipped with bandpass filters appropriate for Alexa Fluor 488 (535/40 nm) and 7-AAD (630/60 nm) fluorescence. The two-color dot plots of annexin V vs. 7-AAD, and the brightfield, combined fluorescence, and darkfield microscopic images are shown.

and integrates signal from each object for 10 milliseconds, allowing the detection of even faint fluorescent probes within cell images that are acquired at high speed. Careful attention to the design of the pump and fluidic system to achieve highly laminar, nonpulsatile flow eliminates any cell rotation or lateral translation on the time scale of the imaging process (35).

Every pixel read from the CCD is analyzed by a real-time algorithm that detects the presence of object images and calculates a number of basic morphometric and photometric features, which can be used as criteria for data storage. Data files encompassing 10,000–20,000 cells are typically about 100 MB in size and are routinely stored and analyzed using standard personal computers. Because the TDI readout process operates continuously and without any "dead time," every cell can be imaged and the coincidental imaging of two or more cells at a time, as depicted in Figure 1, presents no barrier to data acquisition.

Cell Culture and Induction of Cell Death

The human acute T leukemic Jurkat cell line was obtained from ATCC (Rockville, MD; catalog number CRL-1990) and maintained in RPMI 1640 (Gibco, Grand Island, NY) containing 5% fetal bovine serum, 1 mM sodium pyruvate (Mediatech, Herndon, VA), 100 μM nonessential amino acids, 100 U/ml penicillin, 100 μg/ml streptomycin, and 2 mM L-glutamine (BioWhittaker, Walkersville, MD) in 5% CO_2 atmosphere at 37°C. The density of exponentially growing cells was less than 3×10^5 cells per ml at the time of all treatments. To induce necrosis, cells were treated for 1 h with 0.3% hydrogen peroxide (Sigma, St. Louis, MO). To induce early and late apoptosis, cells were treated for 18 h with 1 μM camptothecin (CPT; Sigma), a DNA topoisomerase I inhibitor.

Cell Staining

Control, apoptotic, and necrotic treatment groups were counted and washed once in phosphate buffered saline (PBS; Fisher Scientific, Fair Lawn, NJ). The cells were resuspended at 10^7 cells/ml in Annexin V Binding Buffer (BD Pharmingen, San Diego, CA) containing Alexa Fluor 488 annexin V (Molecular Probes, Eugene, Oregon) and 10 μM 7-aminoactinomycin D (7-AAD, Molecular Probes) for 10 min at room temperature. Necrotic cells were additionally stained with PE anti-HLA-A,B,C (clone G46-2.6, anti-HLA class I; BD Pharmingen). The cells were washed in Annexin V Binding Buffer, fixed in 2% paraformaldehyde (Sigma), and analyzed as either single populations or as a mixture by flow cytometry and immunofluorescence microscopy.

Flow Cytometry and Immunofluorescence Microscopy

For immunofluorescence microscopy, fixed control and treated cells were placed on a conventional glass slide (Erie Scientific, Portsmouth, NH), mixed 1:1 with Antifade (Molecular Probes) and covered with a cover slip. The cells were visualized at 400× using an Eclipse E600 (Nikon, Melville, NY) fluorescence microscope equipped with filters appropriate for Alexa Fluor 488 (535/40 nm emission) and 7-AAD (630/60 nm emission). For flow cytometry, cell fluorescence data excited by a 488-nm laser were acquired using the FACSort™ cytometer (BD Immunocytometry Systems, San Jose, CA) and analyzed using CellQuest™ (BD Immunocytometry Systems). For imaging flow cytometry, fixed cells at 5×10^7 cells per ml were run at 100 cells per second on a "Beta" version of the ImageStream100™ and the data was analyzed using the ImageStream Data Analysis and Exploration Software (IDEAS).

RESULTS

To evaluate the capabilities of data acquired using the ImageStream, and its analysis using the IDEAS software, we undertook analysis of a heterogeneous population of cells that had been induced to undergo both apoptotic and necrotic mechanisms of death. Thus, Jurkat T cells were treated with either peroxide (to induce necrosis) or CPT (to induce apoptosis; this population contained cells in both early and late stages of apoptosis), or were untreated. The three cell populations were then stained with Alexa Fluor 488 annexin V and 7-AAD and evaluated by brightfield, darkfield, and fluorescence microscopy and by conventional flow cytometry (Fig. 2). The vast majority (>98%) of untreated cells were viable at the time of staining and were annexin V^-, 7-AAD^- (double negative, DN; Fig. 2A). CPT treatment resulted in the appearance of both annexin V single positive (SP) early apoptotic cells and annexin V, 7-AAD double positive (DP) late apoptotic cells (Fig. 2B). Similar to late apoptotic cells, peroxide-treated necrotic cells stained positively with both annexin V and 7-AAD (Fig. 2C). Of note, however, is the fact that the condensed, fragmented nuclei of late apoptotic cells could be easily distinguished from the intact nuclei of necrotic cells by immunofluorescence microscopy. Conversely, apoptotic cells exhibited greater darkfield intensity and texture compared to necrotic cells.

In order to demonstrate the concordance of multispectral imaging flow cytometric data with conventional flow cytometric and microscopic data, a mixture of untreated, apoptotic, and necrotic Jurkat cells (individually prepared as described) were analyzed in parallel by conventional flow cytometry and on an ImageStream 100 Beta system. In this experiment, all cells were stained with Alexa Fluor 488-conjugated annexin V and 7-AAD. Necrotic cells were also stained with PE-conjugated anti-HLA class I before mixing, to distinguish them from advanced apoptotic cells and permit "backgating" under appropriate circumstances. On the ImageStream, each cell was simultaneously imaged in darkfield (488 nm laser side-scatter), green fluorescence (500–550 nm, annexin V channel), orange fluorescence (550–600 nm, PE channel), red fluorescence (600–650 nm, 7-AAD channel), and brightfield (660–720 nm). Cells were grouped into live (DN), early apoptotic (SP), or double positive (DP) populations, based on the total intensities of annexin V and 7-AAD staining. Similar bivariate dot plots of annexin V and 7-AAD staining were obtained in analyses from both the conventional and

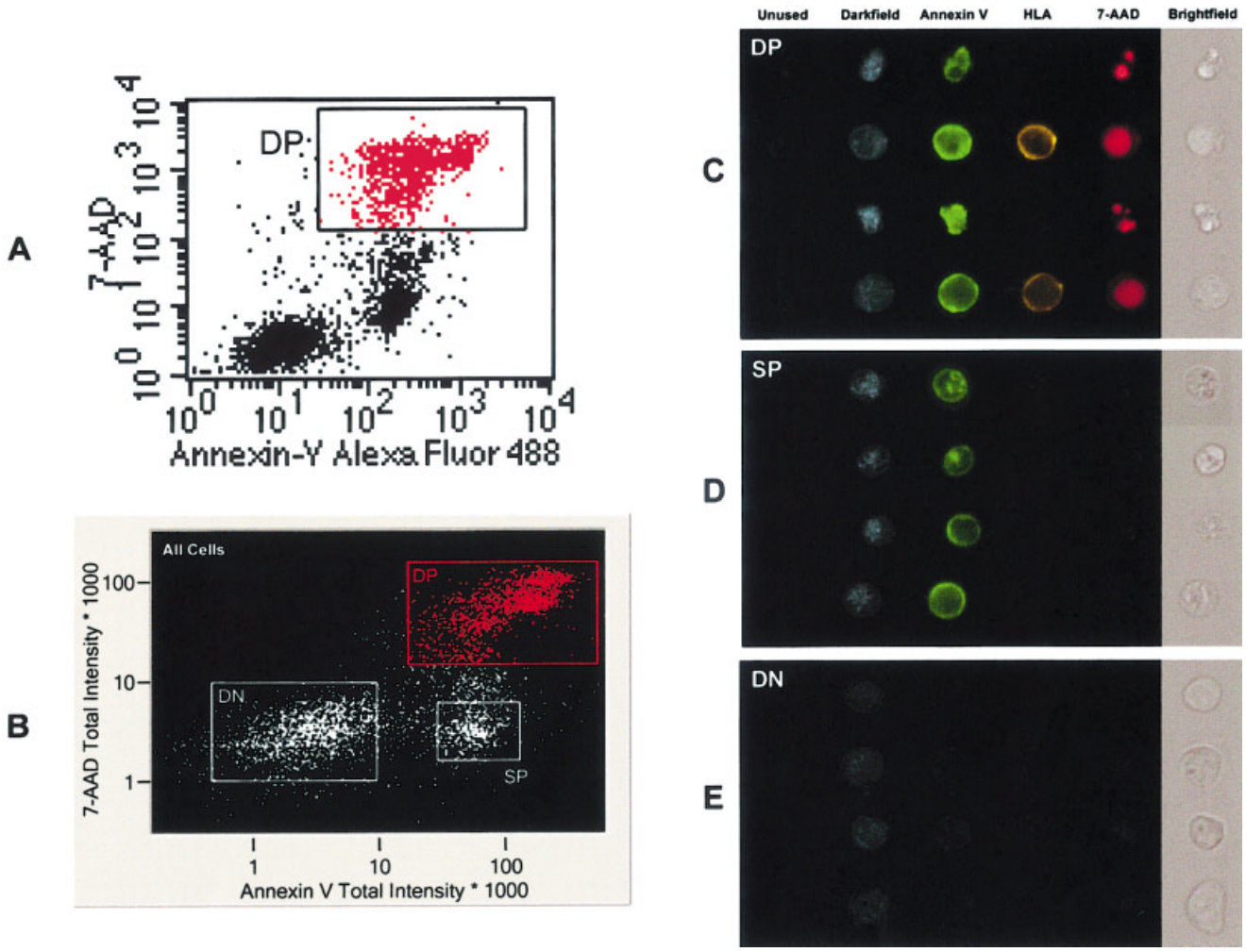

FIG. 3. Flow cytometric imaging of live, apoptotic, and necrotic cells. Untreated, CPT-treated, and peroxide-treated Jurkat cells were stained with Alexa Fluor 488 conjugated annexin V and 7-AAD. Peroxide-treated cells were separately stained with HLA class I-PE to permit "tracking" of cells subjected to the necrosis-inducing treatment. After staining, equal cell numbers of the three populations of cells were mixed and analyzed for annexin V and 7-AAD expression by conventional flow cytometry using a FACSort™ (**A**); and multispectral imaging of cells in flow using an ImageStream 100 cytometer (**B**). **C–E**: The six-channel images of cells from representative members of the double positive (DP), single positive (SP), and double negative (DN) populations identified using the ImageStream 100 are shown in C, D, and E, respectively.

multispectral imaging flow cytometers (Fig. 3A and B, respectively). However, a unique aspect of data collected on the ImageStream system is that each data point can be "clicked on" to observe the cell imagery associated with that data point. In addition, each population gate can be used to perform a "virtual cell sort" by displaying only the images of cells that fall within the gate. Representative images of cells contained in the DP, SP, and DN gates are shown in Figure 3C, D, and E, respectively, with different cells represented by different image rows. Compared to live cells that fall into the DN gate, early apoptotic cells (cells in the SP gate) appear slightly shrunken, with more complex brightfield and darkfield morphologies than cells in the DN gate. The double positive (DP) population contains cells with two distinct morphologies: one containing small, irregularly-shaped cells with condensed, fragmented nuclei; and one containing larger cells with large, unfragmented nuclei that stained uniformly with 7-AAD. The morphology of these two populations of cells are consistent with cells in the late stage of apoptosis and necrosis, respectively.

As noted earlier, although advanced apoptotic and necrotic cells differ morphologically, they cannot be distinguished based solely on annexin V and 7-AAD fluorescence. Plotting the mixed late apoptotic and necrotic DP population on a FSC versus SSC plot reveals two distinct populations of cells (Fig. 4A). Analysis of the DP population of cells obtained on the conventional flow cytometer for staining with PE (which was used to stain only the necrotic subpopulation of cells) permits separation of the necrotic and apoptotic subpopulations of cells (Fig. 4B). Backgating the PE positive necrotic population in blue reveals that the low SSC population consists of necrotic cells (Fig. 4C).

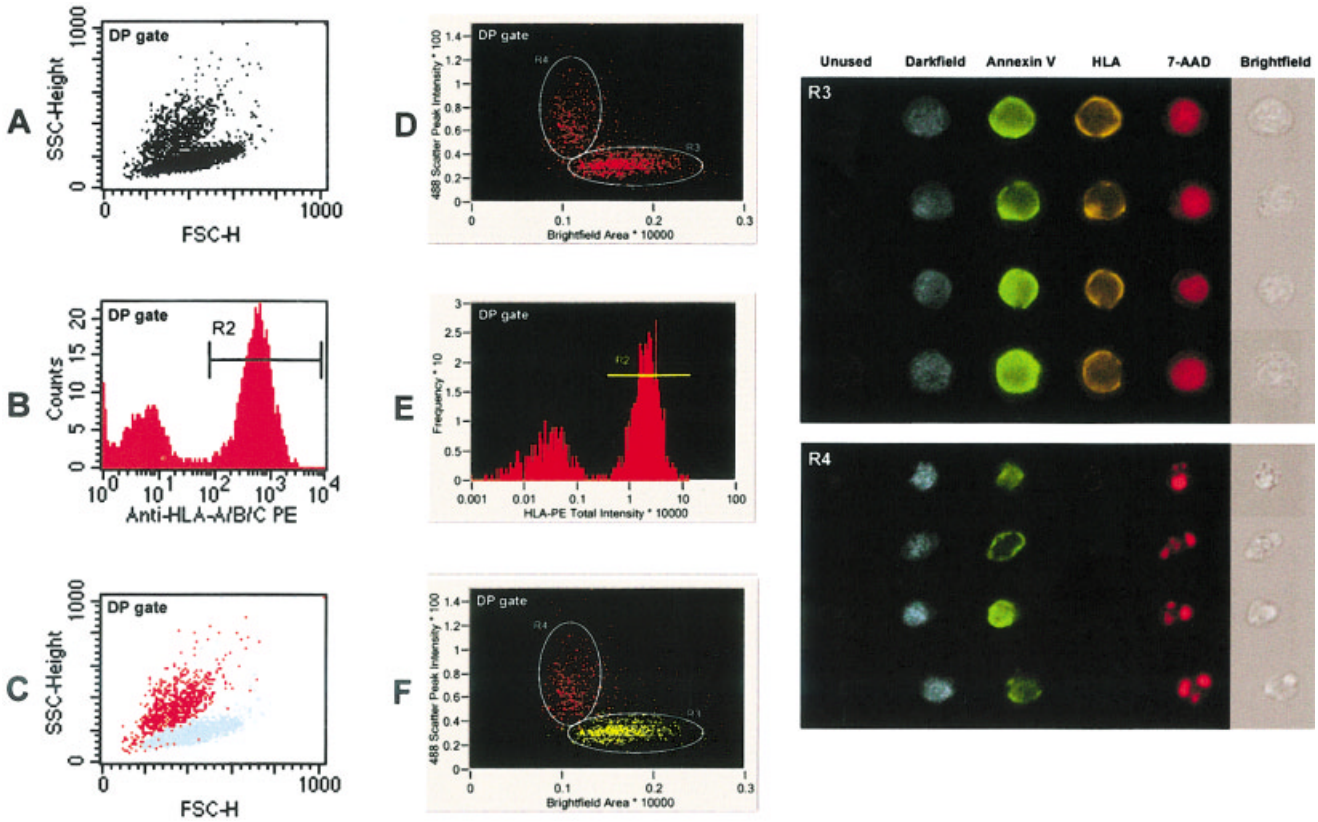

FIG. 4. "Virtual sorting" of cells using morphometric criteria permits resolution of necrotic from late apoptotic cells. **A:** Laser scatter analysis (forward versus side) of the "DP gate" population of cells from Figure 3A performed using CellQuest™ software on data obtained using a FACSort™ cytometer demonstrates two subpopulations of cells. **B:** Single-color histogram of HLA class I-PE on DP cells from Figure 3A as measured using a FACSort cytometer. **C:** Backgating of HLA class I-PE$^+$ cells (B) onto the scatter histogram (A) permits identification of discrete subsets of necrotic and late apoptotic cells. **D:** Bivariate plotting of "Brightfield Area" versus "488-nm Scatter Peak Intensity" performed using IDEAS® software, from data obtained using the ImageStream cytometer, demonstrates two subpopulations of cells. Visual inspection of the images demonstrates that cells in the R3 gate are undergoing necrosis, while cells in the R4 gate are in the late stages of apoptosis. **E:** Single-color histogram of HLA class I-PE on DP cells from Figure 3D as measured using the ImageStream cytometer. **F:** Backgating of peroxide-treated HLA class I-PE$^+$ cells (E) onto the scatter histogram (D) confirms the mechanisms of death (i.e., necrosis versus apoptosis) in cells identified by "virtually sorting" of cells (D). HLA class I-PE$^+$ cells (i.e., peroxide-treated) are shown in red, while HLA class I-PE$^-$ cells (i.e., CPT-treated) are shown in yellow.

As demonstrated above, without imagery or the aid of an extra marker (anti-HLA class I-PE in this case), data obtained from a conventional flow cytometer does not permit us to identify which cells correspond to which population. In contrast, ImageStream fluorescence data is linked to cell imagery, and the morphology of gated populations can be viewed directly. Analysis the DP population for size with IDEAS (brightfield area) and scatter peak intensity (Fig. 4D), also revealed two populations of cells. The nuclei of cells that fell within the high brightfield area, low scatter peak intensity area (R3) were intact, uniformly stained with 7-AAD, and had a morphology consistent with necrotic cells. The nuclei of cells that fell within the low brightfield area, high scatter peak intensity area (R4) were condensed and fragmented, and had a morphology consistent with cells in the late stages of apoptosis. Backgating PE-positive cells (identified in the histogram shown in Fig. 4E), in yellow, verified that R3 gated cells were derived from the necrotic treatment group (Fig. 4F). This conclusion is further supported by morphologic examination of cells in the image galleries of the R3 and R4 gated cells, and confirms that the low area/high texture cells were apoptotic (HLA-class I PE$^-$ cells containing fragmented 7-AAD staining nuclei; lower right gallery), while high area/low texture cells were necrotic (HLA class I-PE$^+$ cells containing uniform 7-AAD staining nuclei; upper right gallery).

A unique aspect of multispectral image data collection is that it not only enables calculation of standard intensity-based parameters and statistics employed in conventional flow cytometry, but also permits quantitation of numerous other morphologic features (e.g., cell area, perimeter, aspect ratio, texture, spot counts, cell centroid, gradient intensity, and spatial frequency). Using this capability it is possible to distinguish all four cell populations (i.e., live, early apoptotic, late apoptotic, and necrotic) in a single step using morphologic features derived from 7-AAD, brightfield, and darkfield imagery, and in the absence of other staining procedures often used to "identify" apoptotic cells. By subtracting the 7-AAD image area (nuclear

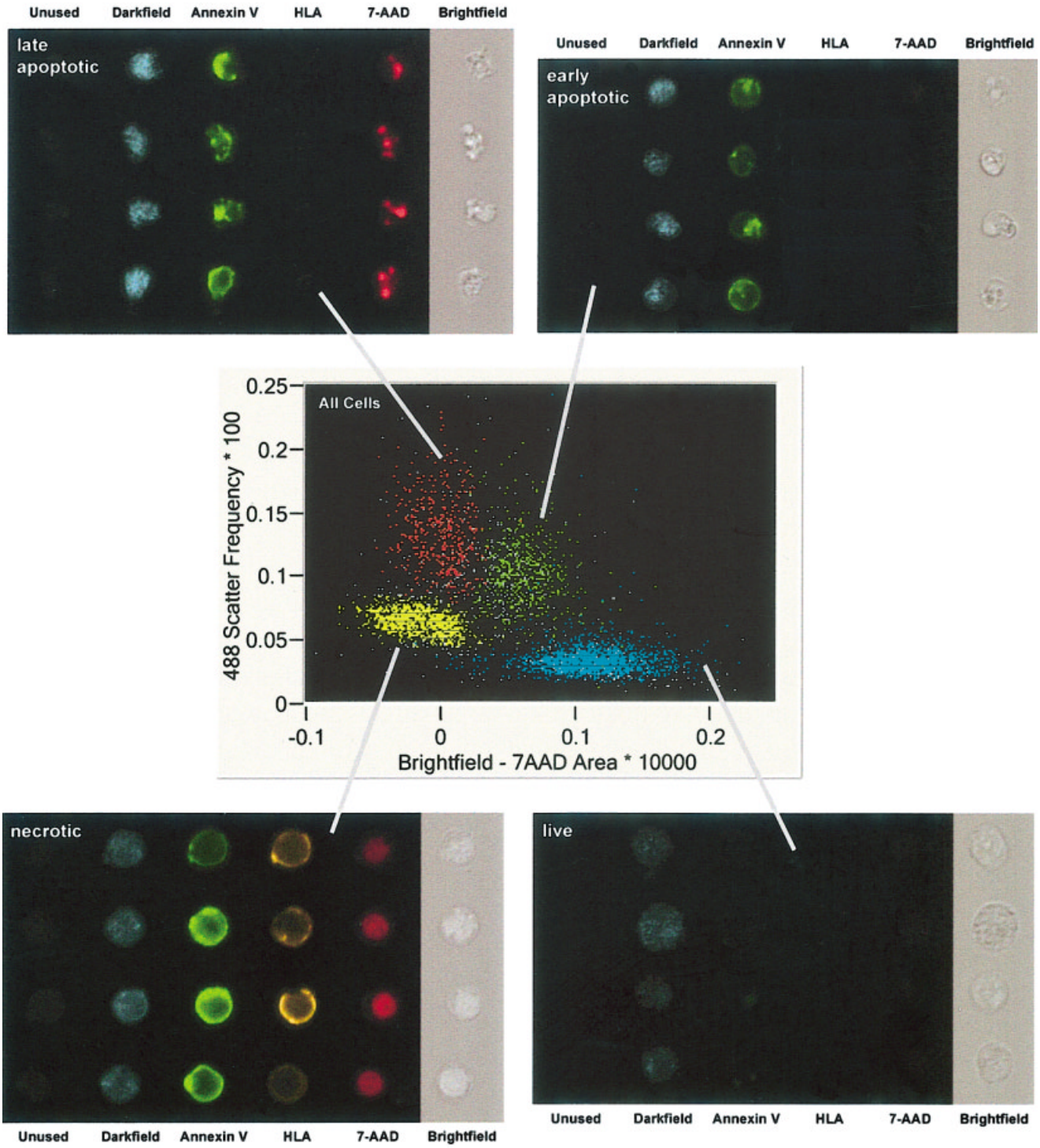

FIG. 5. Resolution of live, early and late apoptotic, and necrotic cells using morphometric features based on scatter intensity, brightfield area, and nuclear area. Calculation of a complex morphometric feature using the IDEAS software to estimate cytoplasmic area of a cell was performed by subtracting the nuclear area (as defined by 7-AAD staining) from the total cellular area (as defined by Brightfield area). A bivariate plot of cells contained in the "All Cells" gate (which contained live cells, early and late apoptotic cells, and necrotic cells) revealed four distinguishable subpopulations of cells. Visual inspection of cells contained in these subpopulations demonstrated that the live cells lie in the lower right quadrant (i.e., cytoplasmic area^{hi}, scatter^{lo}), early apoptotic cells lie in the upper right quadrant (i.e., cytoplasmic area^{hi}, scatter^{hi}), late apoptotic cells lie in the upper left quadrant (i.e., cytoplasmic area^{lo}, scatter^{hi}), and necrotic cells lie in the lower left quadrant (i.e., cytoplasmic area^{lo}, scatter^{lo}). Backgating of the four cell populations that had been identified using alternative criteria confirmed their identity with live cells and early apoptotic cells with the DN and SP cells shown in Figure 3B (shown in blue and green, respectively), and with the necrotic and late apoptotic cells with cells contained in gates R3 and R4 shown in Figure 4 (shown in yellow and red, respectively).

size) from the brightfield area (cell size) we obtain a value that is an indication of cytoplasmic size. When this complex morphologic feature (here named "Brightfield - 7-AAD Area") was used in conjunction with a feature derived from the darkfield imagery (i.e., 488 nm spatial scatter frequency) four subpopulations of cells become evident (Fig. 5). Live cells (depicted in blue) excluded the cell-impermeant 7-AAD fluorescent DNA binding dye, which minimized the nuclear image area and resulted in cells with a large calculated cytoplasmic area. Early apoptotic cells (shown in green) are just as effective as live cells at excluding 7-AAD, but their total brightfield area is slightly smaller due to the early stages of cytoplasmic blebbing, thereby resulting in an intermediate value for the "Brightfield - 7AAD Area" parameter. Also associated with the early stages of apoptosis is a significant increase in 488-nm scatter peak intensity that clearly separates these cells from live cells on the vertical axis of the dot plot. Both necrotic cells (depicted in yellow) and late apoptotic cells (depicted in red) had compromised membrane integrity, which permits free entry of 7-AAD and thus strong nuclear images of relatively large areas, shifting these populations to the left on the dot plot. However, these two cell populations can be clearly separated based on the peak intensity measurements derived from their 488-nm scatter parameters. Necrotic cells produce darkfield images of relatively low complexity compared to the more complex and heterogeneous darkfield images of apoptotic cells, thus clearly separating the two populations in the vertical axis. Inspection of the associated image galleries associated with these four gated populations of cells confirmed the classification of each population.

DISCUSSION

This study demonstrated the ability of the ImageStream multispectral imaging flow cytometer to correctly identify distinct modes of cell death using various combinations of fluorescence intensity and image morphometry measurements. Multispectral imaging of cells in flow was first used to recapitulate a standard flow cytometric apoptosis assay, identifying live, early apoptotic, and late apoptotic/necrotic populations using fluorescence intensity measurements derived from images of 7-AAD and annexin V stained cells. The identities of cell populations were verified using the "virtual cell sort" function of the IDEAS data analysis software, by inspecting the brightfield, fluorescence, and darkfield (laser side-scatter) imagery obtained from each cell. The morphology was consistent with brightfield, fluorescence, and darkfield images obtained using standard microscopy. Subsequently, the multispectral image data were used to resolve the late apoptotic from necrotic populations based on the differences in brightfield area and darkfield peak intensity between the two populations. This morphologic classification was then verified using an HLA marker present only on the necrotic cell population. Finally, a complex morphologic feature ("Brightfield - 7-AAD Area") was defined and combined with the darkfield peak intensity feature to allow a single-step morphometric classification of live, early apoptotic, late apoptotic, and necrotic cell populations without reference to the annexin V signal. By providing comprehensive multispectral imagery of each cell along with all the photometric features of flow cytometry, multispectral imaging in flow allows for discrimination of cell types not feasible with standard flow cytometry.

LITERATURE CITED

1. Jacobson MD, Weil M, Raff MC. Programmed cell death in animal development. Cell 1997;88:347–354.
2. Rathmell JC, Thompson CB. Pathways of apoptosis in lymphocyte development, homeostasis, and disease. Cell 2002;109(suppl):S97–S107.
3. Vaux DL, Korsmeyer SJ. Cell death in development. Cell 1999;96: 245–254.
4. Ashkenazi A, Dixit VM. Death receptors: signaling and modulation. Science 1998;281:1305–1308.
5. Thompson CB. Apoptosis in the pathogenesis and treatment of disease. Science 1995;267:1456–1462.
6. Fadeel B, Orrenius S, Zhivotovsky B. The most unkindest cut of all: on the multiple roles of mammalian caspases. Leukemia 2000;14:1514–1525.
7. Ormerod MG, Collins MK, Rodriguez-Tarduchy G, Robertson D. Apoptosis in interleukin-3-dependent haemopoietic cells. Quantification by two flow cytometric methods. J Immunol Methods 1992;153:57–65.
8. Castedo M, Ferri K, Roumier T, Metivier D, Zamzami N, Kroemer G. Quantitation of mitochondrial alterations associated with apoptosis. J Immunol Methods 2002;265:39–47.
9. Green D, Kroemer G. The central executioners of apoptosis: caspases or mitochondria? Trends Cell Biol 1998;8:267–271.
10. Green DR, Reed JC. Mitochondria and apoptosis. Science 1998;281: 1309–1312.
11. Kroemer G, Reed JC. Mitochondrial control of cell death. Nat Med 2000;6:513–519.
12. Lizard G, Fournel S, Genestier L, Dhedin N, Chaput C, Flacher M, Mutin M, Panaye G, Revillard JP. Kinetics of plasma membrane and mitochondrial alterations in cells undergoing apoptosis. Cytometry 1995;21:275–283.
13. Komoriya A, Packard BZ, Brown MJ, Wu ML, Henkart PA. Assessment of caspase activities in intact apoptotic thymocytes using cell-permeable fluorogenic caspase substrates. J Exp Med 2000;191:1819–1828.
14. Smolewski P, Grabarek J, Halicka HD, Darzynkiewicz Z. Assay of caspase activation in situ combined with probing plasma membrane integrity to detect three distinct stages of apoptosis. J Immunol Methods 2002;265:111–121.
15. Lecoeur H, de Oliveira-Pinto LM, Gougeon ML. Multiparametric flow cytometric analysis of biochemical and functional events associated with apoptosis and oncosis using the 7-aminoactinomycin D assay. J Immunol Methods 2002;265:81–96.
16. van Engeland M, Nieland LJ, Ramaekers FC, Schutte B, Reutelingsperger CP. Annexin V-affinity assay: a review on an apoptosis detection system based on phosphatidylserine exposure. Cytometry 1998; 31:1–9.
17. Vermes I, Haanen C, Steffens-Nakken H, Reutelingsperger C. A novel assay for apoptosis. Flow cytometric detection of phosphatidylserine expression on early apoptotic cells using fluorescein labelled Annexin V. J Immunol Methods 1995;184:39–51.
18. Koopman G, Reutelingsperger CP, Kuijten GA, Keehnen RM, Pals ST, van Oers MH. Annexin V for flow cytometric detection of phosphatidylserine expression on B cells undergoing apoptosis. Blood 1994; 84:1415–1420.
19. Verhoven B, Schlegel RA, Williamson P. Mechanisms of phosphatidylserine exposure, a phagocyte recognition signal, on apoptotic T lymphocytes. J Exp Med 1995;182:1597–1601.
20. Gaforio JJ, Serrano MJ, Algarra I, Ortega E, Alvarez de Cienfuegos G. Phagocytosis of apoptotic cells assessed by flow cytometry using 7-aminoactinomycin D. Cytometry 2002;49:8–11.
21. Ormerod MG, Sun XM, Snowden RT, Davies R, Fearnhead H, Cohen GM. Increased membrane permeability of apoptotic thymocytes: a flow cytometric study. Cytometry 1993;14:595–602.
22. Schmid I, Uittenbogaart CH, Keld B, Giorgi JV. A rapid method for measuring apoptosis and dual-color immunofluorescence by single laser flow cytometry. J Immunol Methods 1994;170:145–157.
23. Philpott NJ, Turner AJ, Scopes J, Westby M, Marsh JC, Gordon-Smith EC, Dalgleish AG, Gibson FM. The use of 7-amino actinomycin D in

identifying apoptosis: simplicity of use and broad spectrum of application compared with other techniques. Blood 1996;87:2244–2251.
24. Alnemri ES, Livingston DJ, Nicholson DW, Salvesen G, Thornberry NA, Wong WW, Yuan J. Human ICE/CED-3 protease nomenclature. Cell 1996;87:171.
25. Kohler C, Orrenius S, Zhivotovsky B. Evaluation of caspase activity in apoptotic cells. J Immunol Methods 2002;265:97–110.
26. Gong J, Traganos F, Darzynkiewicz Z. A selective procedure for DNA extraction from apoptotic cells applicable for gel electrophoresis and flow cytometry. Anal Biochem 1994;218:314–319.
27. Gorczyca W, Bigman K, Mittelman A, Ahmed T, Gong J, Melamed MR, Darzynkiewicz Z. Induction of DNA strand breaks associated with apoptosis during treatment of leukemias. Leukemia 1993;7:659–670.
28. Gorczyca W, Gong J, Darzynkiewicz Z. Detection of DNA strand breaks in individual apoptotic cells by the in situ terminal deoxynucleotidyl transferase and nick translation assays. Cancer Res 1993;53: 1945–1951.
29. Lecoeur H, Prevost MC, Gougeon ML. Oncosis is associated with exposure of phosphatidylserine residues on the outside layer of the plasma membrane: a reconsideration of the specificity of the annexin V/propidium iodide assay. Cytometry 2001;44:65–72.
30. Kerr JF, Wyllie AH, Currie AR. Apoptosis: a basic biological phenomenon with wide-ranging implications in tissue kinetics. Br J Cancer 1972;26:239–257.
31. Darzynkiewicz Z, Juan G, Li X, Gorczyca W, Murakami T, Traganos F. Cytometry in cell necrobiology: analysis of apoptosis and accidental cell death (necrosis). Cytometry 1997;27:1–20.
32. Tarnok A, Gerstner AO. Clinical applications of laser scanning cytometry. Cytometry 2002;50:133–143.
33. Ortyn WE, Basiji DA. Imaging and analyzing parameters of small moving objects. USA patent 6249341. 2001.
34. Basiji DA, Ortyn WE. Imaging and analyzing parameters of small moving objects. USA patent 6211955. 2001.
35. Ortyn WE, Basiji DA, Bauer RA, Frost KL, Perry DJ, Riley JK. Measuring the velocity of small moving objects such as cells. USA patent 6532061. 2003.
36. Valet G, Leary JF, Tárnok A. Cytomics—new technologies: towards a human cytome project. Cytometry 2004;59A:167–171.